Accurate measurement of the surface residual stresses generated by milling in pre-equilibrium state

Longhui Meng,[b] Maen Atli,[c] Yinfei Yang,[a] and Ning He
College of Mechanical and Electrical Engineering, Nanjing University of Aeronautics and Astronautics, Nanjing, Jiangsu 210016, China

(Received 22 January 2016; accepted 25 April 2016)

We introduce a method to measure accurately surface residual stresses in the pre-equilibrium state, which were generated in workpieces during the milling process. The method takes into account strain changes and uses the inverse calculation. Material in the stress layer was removed layer by layer, and the strain change on the opposite side of the machined surface was measured. We also consider the change of the bending moment caused by the changed neutral layer. The stress values were calculated from the last layer to the first layer, and the residual stresses generated by milling are measured. We created a finite element model of a real workpiece and the measured stress values were used as inputs for the model. The measuring method was validated using finite element analysis. We find that our measuring method can be successfully used in practice to measure surface residual stresses and it provides reliable indicators for evaluating the surface properties of machined workpieces.

I. INTRODUCTION

Residual stresses significantly affect fatigue life, geometrical stability, corrosion resistance and crack resistance of machined workpieces.[1,2] Surface residual stresses occur due to severe inelastic (plastic) deformations caused by high temperatures, high pressures, high strain rates, thermal gradients, and phase transformations during the machining process.[3] The depth of the stress layer is very shallow. Most of the time it is less than 0.2 mm, but the stress gradients within the stress layers are often very large.

Since the 1930s, over ten different methods have been developed to measure residual stresses. The methods can be divided into two main categories: destructive and nondestructive. The destructive methods include center-hole drilling, ring-core, deep-hole, sectioning, and contour. Among these, the center-hole drilling method is most commonly used. The nondestructive techniques include the Barkhausen noise method, x-ray diffraction (XRD), neutron diffraction, and ultrasonic tests. The most commonly used among these is XRD.[4–7]

Based on the characteristics of surface residual stresses induced by machining, to date, the most commonly used measurement procedure involves a combination of the XRD method and layer removal.[3,8] As a result, they cannot include the initial states of the residual stresses induced by the machining process or predict the deformations of workpiece with different rigidities. This can be explained, as the final state of the surface residual stresses will go through two phases. First, the surface residual stresses in pre-equilibrium state are caused by many factors during the machining process. Second, the surface residual stresses are redistributed to achieve an equilibrium state, which will cause some deformations of the workpiece—see Fig. 1. The stress values obtained with the XRD method are the values in the equilibrium state. They are always affected by the rigidity of the workpiece, so they cannot represent stress values in workpieces with different rigidities. Furthermore, they cannot predict the corresponding deformations of the workpiece caused by the surface residual stresses. In other studies, the nano indentation technique was used to examine the surface residual stresses. However, it is almost impossible to obtain the relationship between the stress values and the depth in the machined surface using this technique.[9,10]

In this paper, we describe a measuring method based on the strain changes due to stress layer removal and inverse calculations. It enables us to obtain the surface residual stresses changing through the depth into the machined surface in the pre-equilibrium state. So obtained stress values eliminate the influence of workpiece rigidity. Both the corresponding deformations of the workpieces with different rigidities and the final states of the surface residual stresses can be predicted based on the residual stresses in the pre-equilibrium state.

Contributing Editor: Jürgen Eckert
Address all correspondence to these authors.
[a]e-mail: yyfgoat@nuaa.edu.cn
[b]e-mail: menglonghui@nuaa.edu.cn
[c]e-mail: maen_atly@yahoo.com
DOI: 10.1557/jmr.2016.205

II. MEASURING THEORY AND METHOD

E. Brinksmeier proposed a similar residual stress measuring method based on the maximal deviation *PV* of the aerospace component.[11] The maximum deviation *PV* can be obtained based on the beam theory as:

$$PV = -\frac{M \cdot l^2}{8 \cdot E \cdot I} \quad , \tag{1}$$

where M is the bending moment caused by the residual stresses, l and I are the length and second moment of inertia of the component, respectively. The bending moment M can be calculated by integrating the source stresses along the penetration depth z_0 as:

$$M = \int_0^{Z_0} b \cdot \sigma \cdot \left(z - \frac{h}{2}\right) \mathrm{d}z \quad , \tag{2}$$

where b is the beam width along which the residual stresses are assumed to be constant; h is the beam thickness; z_0 is the penetration depth of the residual stress.

The residual force can be calculated as:

$$F' = \sigma \cdot z_0 = -\frac{16 \cdot PV \cdot E \cdot I}{(z_0 - h) \cdot b \cdot l^2} \quad . \tag{3}$$

The measuring results of the stress values obtained based on Eqs. (1) and (2) are not very accurate in some cases, which can be attributed to two factors: firstly, the measuring theory just considers the residual stresses along the length of the component, while the residual stresses vertical to that direction will also affect the maximal deviation *PV*. Secondly, the maximal deviation *PV* caused by residual force is very different from that caused by external force. Furthermore, different states of the residual stresses were not considered either.

Although different methods for measuring the surface residual stresses induced by machining were proposed by the authors in Refs. 12–16, for the measurement of the residual stresses generated by milling, only the stresses in cutting direction were considered. They were obtained based on the changes of the workpiece bending deflection due to the stress layers removal. In this study, not only the residual stresses in the cutting direction, but also the residual stresses in the transverse direction are considered. It is based on the strain changes on the surface opposite to the machined surface during the stress layers removal. This is much more complex because the stresses in one direction affect the strains in different directions. The schematic of a milled workpiece is shown in Fig. 2. The red surface is the milled surface, and there are residual stresses generated by milling in the surface layer.

The strain gauges are attached to the surface opposite the machined surface to measure the strains in both the cutting and the transverse directions, as shown in Fig. 3. The cutting direction is set as the x direction, and the transverse direction is set as y direction. Because the thickness of the surface stress layer is very thin, to

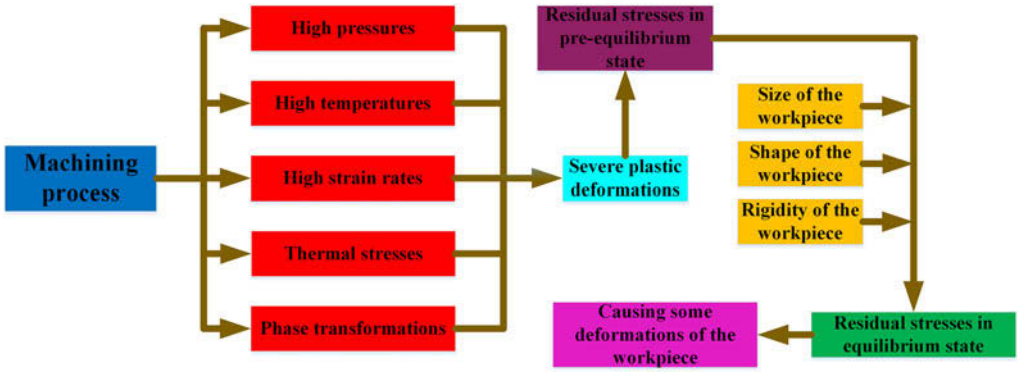

FIG. 1. The formation of the final state of machining induced residual stresses.

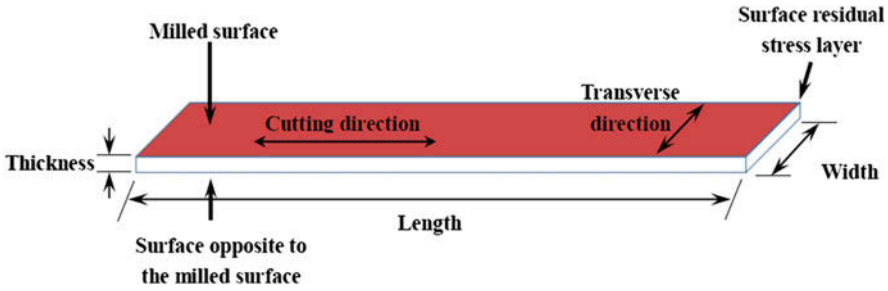

FIG. 2. Schematic of the milled workpiece and the corresponding surface residual stress layer.

measure the residual stresses through the thickness, the material in the surface residual stress layer needs to be removed layer by layer.

The deformation of the workpiece caused by the residual stresses not only depends on the stress in each layer but also on the distance from the neutral layer. Because the neutral layer always remains in the middle layer of the workpiece, the position of the neutral layer changes after each layer removal. Therefore, the changes of the deformation of the workpiece are not only affected by the release of the residual stresses in the removed layer, but also by the changed neutral layer and the residual stresses in the remaining layers. Assuming there is no strain change after the nth layer removal, the surface residual stress layer can be considered as completely removed. The flow chart of removing the material layer by layer is shown in Fig. 4.

However, after the removal of the nth layer, because there are no remaining stress layers, we attribute the change of the deformation of the workpiece to the release of the residual stresses in the nth layer. The calculation of the through thickness residual stresses can be started from the nth layer, which is also the last removed stress layer. The flow chart of calculating the residual stresses layer by layer is as shown in Fig. 5.

The thickness of the nth layer is h_n, the thickness of the workpiece after the removal of the nth layer is H, see Fig. 6.

The stress value in one direction in each layer is assumed the same. In the equilibrium state, before the removal of the nth layer, the stresses in x and y directions in the neutral layer can be expressed as:

$$\sigma^n_{xx0} = -\frac{\sigma^n_x \cdot h_n}{H + h_n} \quad , \tag{4}$$

$$\sigma^n_{yy0} = -\frac{\sigma^n_y \cdot h_n}{H + h_n} \quad . \tag{5}$$

Here σ^n_x and σ^n_y are the residual stresses in the nth layer in the pre-equilibrium state. The strains in the neutral layer are:

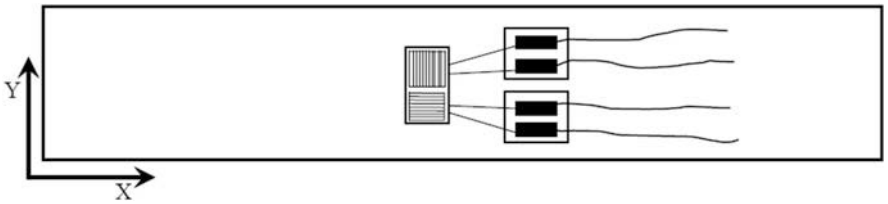

FIG. 3. Schematic of the strain gauges attached to the surface opposite the milled surface.

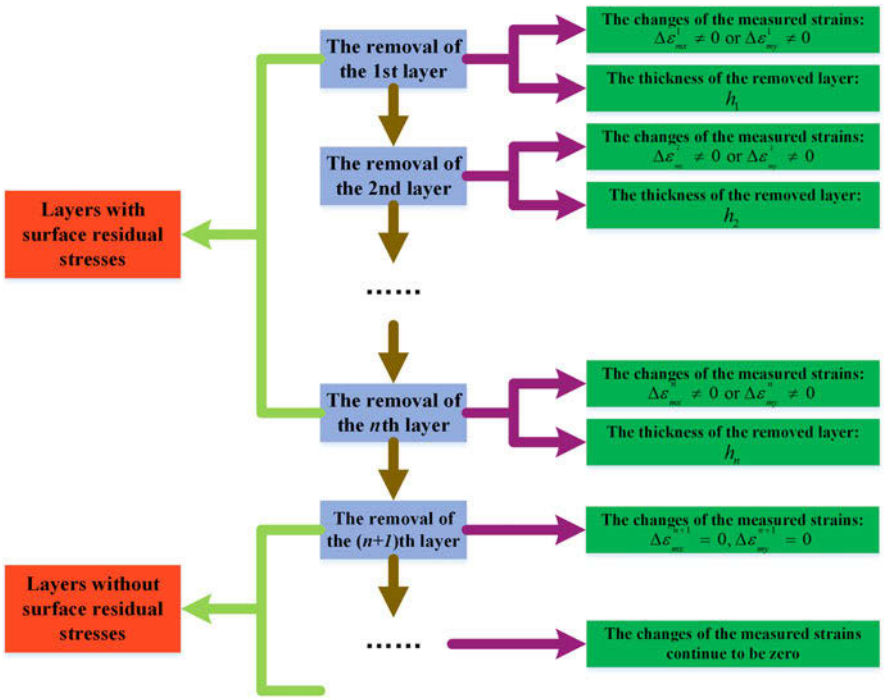

FIG. 4. The flow chart of removing the material, layer by layer.

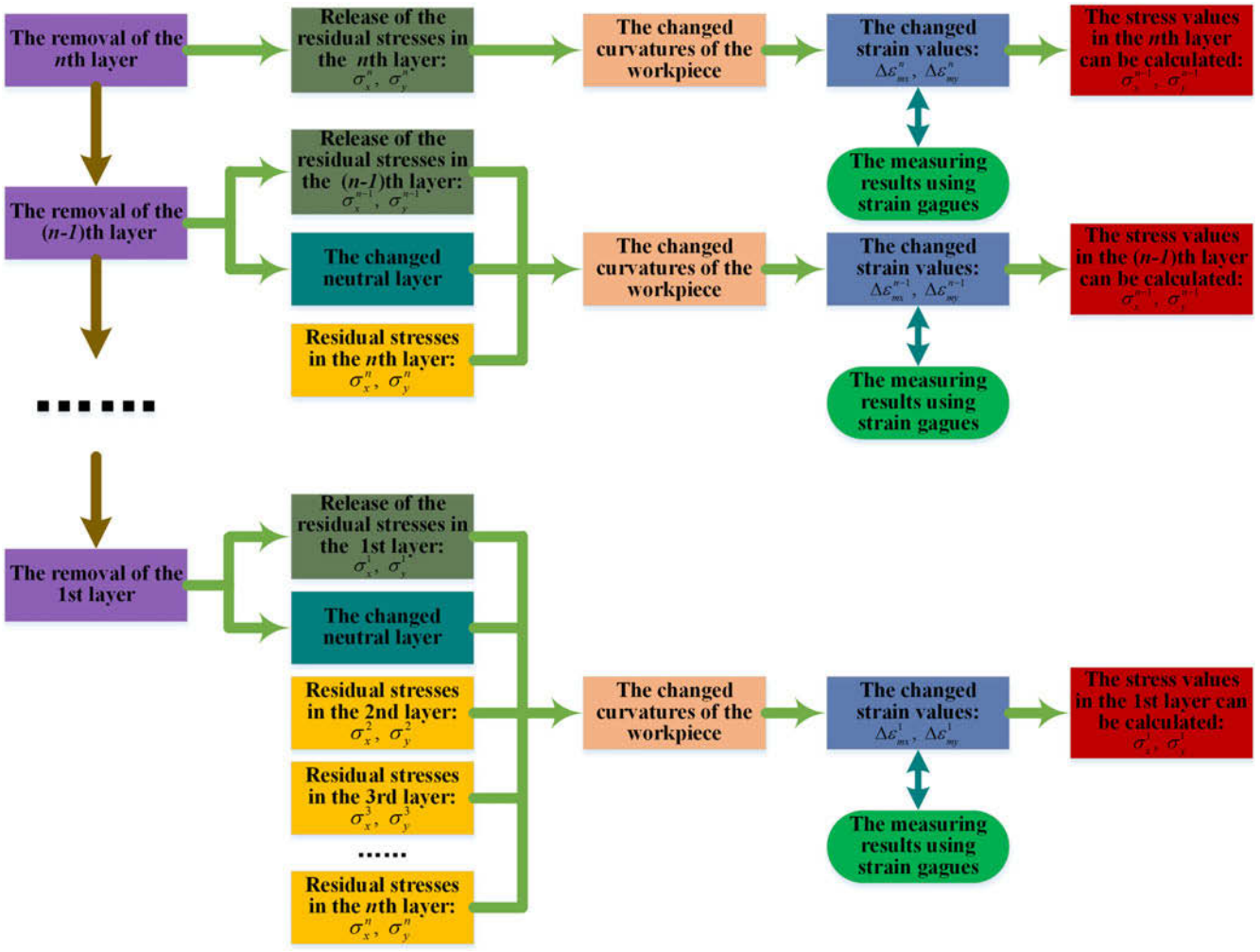

FIG. 5. The flow chart for calculating the residual stresses layer by layer.

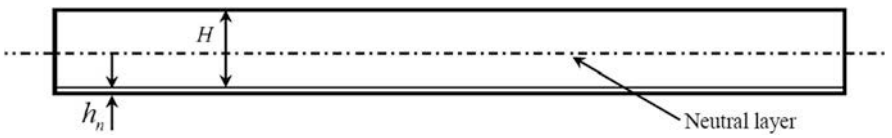

FIG. 6. Schematic of the workpiece with the last unremoved layer.

$$\varepsilon_{xx0}^n = \frac{1}{E}\left(\sigma_{xx0}^n - \mu\cdot\sigma_{yy0}^n\right) \quad , \tag{6}$$

$$\varepsilon_{yy0}^n = \frac{1}{E}\left(\sigma_{yy0}^n - \mu\cdot\sigma_{xx0}^n\right) \quad . \tag{7}$$

Here E and μ are the elastic modulus and Poisson's ratio of the workpiece material. The curvatures of the workpiece in x and y directions are defined as ρ_x^n and ρ_y^n, respectively. Hence, the strains through the thickness of the workpiece can be written as:

$$\varepsilon_x^n(z) = \rho_x^n\cdot z + \varepsilon_{xx0}^n \quad , \tag{8}$$

$$\varepsilon_y^n(z) = \rho_y^n\cdot z + \varepsilon_{yy0}^n \quad . \tag{9}$$

Here z is the coordinate in the depth direction; z is defined as 0 in the neutral layer. When an equilibrium state is obtained, the stresses in the nth layer are:

$$\sigma_x^n(z)' = \sigma_x^n + E'\left[\varepsilon_x^n(z) + \mu\cdot\varepsilon_y^n(z)\right] \quad , \tag{10}$$

$$\sigma_y^n(z)' = \sigma_y^n + E'\left[\varepsilon_y^n(z) + \mu\cdot\varepsilon_x^n(z)\right] \quad . \tag{11}$$

Where $E' = E/1-\mu^2$, the stresses in the remaining part of the workpiece can be expressed as:

$$\sigma_x^n(z)' = E'\left[\varepsilon_x^n(z) + \mu \cdot \varepsilon_y^n(z)\right] \quad , \tag{12}$$

$$\sigma_y^n(z)' = E'\left[\varepsilon_y^n(z) + \mu \cdot \varepsilon_x^n(z)\right] \quad . \tag{13}$$

Because the total bending moment caused by the residual stresses in the workpiece in the equilibrium state is 0, the bending moments in x and y directions are:

$$M_x^n = \int_{-\frac{H+h_n}{2}}^{\frac{H+h_n}{2}} \sigma_x^n(z)' \cdot z \cdot \mathrm{d}z = 0 \quad , \tag{14}$$

$$M_y^n = \int_{-\frac{H+h_n}{2}}^{\frac{H+h_n}{2}} \sigma_y^n(z)' \cdot z \cdot \mathrm{d}z = 0 \quad . \tag{15}$$

According to Eqs. (10)–(13), the bending moments are:

$$M_x^n = \int_{-\frac{H+h_n}{2}}^{-\frac{H-h_n}{2}} \sigma_x^n \cdot z \cdot \mathrm{d}z + \int_{-\frac{H+h_n}{2}}^{\frac{H+h_n}{2}} E'\left[\varepsilon_x^n(z) + \mu \cdot \varepsilon_y^n(z)\right] \cdot z \cdot \mathrm{d}z = 0 \quad , \tag{16}$$

$$M_y^n = \int_{-\frac{H+h_n}{2}}^{-\frac{H-h_n}{2}} \sigma_y^n \cdot z \cdot \mathrm{d}z + \int_{-\frac{H+h_n}{2}}^{\frac{H+h_n}{2}} E'\left[\varepsilon_y^n(z) + \mu \cdot \varepsilon_x^n(z)\right] \cdot z \cdot \mathrm{d}z = 0 \quad . \tag{17}$$

Based on the above, the relationship between the curvatures and the stresses in x and y direction in the nth layer are:

$$E'\left(\rho_x^n + \mu \cdot \rho_y^n\right) \cdot (H + h_n)^3 = 6 \cdot \sigma_x^n \cdot H \cdot h_n \quad , \tag{18}$$

$$E'\left(\rho_y^n + \mu \cdot \rho_x^n\right) \cdot (H + h_n)^3 = 6 \cdot \sigma_y^n \cdot H \cdot h_n \quad . \tag{19}$$

The changes of the measured strains after the removal of the nth layer are:

$$\Delta\varepsilon_{mx}^n = -\frac{\rho_x^n \cdot (H + h_n)}{2} - \varepsilon_{xx0}^n \quad , \tag{20}$$

$$\Delta\varepsilon_{my}^n = -\frac{\rho_y^n \cdot (H + h_n)}{2} - \varepsilon_{yy0}^n \quad . \tag{21}$$

Now the curvatures of the workpiece before the removal of the nth layer can be calculated based on the changes of the measured strains:

$$\rho_x^n = -\frac{2\left(\Delta\varepsilon_{mx}^n + \varepsilon_{xx0}^n\right)}{H + h_n} \quad , \tag{22}$$

$$\rho_y^n = -\frac{2\left(\Delta\varepsilon_{my}^n + \varepsilon_{yy0}^n\right)}{H + h_n} \quad . \tag{23}$$

Based on Eqs. (18), (19), (22) and (23), the residual stresses in the nth layer are:

$$\sigma_x^n = \frac{E'\left(\rho_x^n + \mu \cdot \rho_y^n\right) \cdot (H + h_n)^3}{6 \cdot H \cdot h_n} \quad , \tag{24}$$

$$\sigma_y^n = \frac{E'\left(\rho_y^n + \mu \cdot \rho_x^n\right) \cdot (H + h_n)^3}{6 \cdot H \cdot h_n} \quad . \tag{25}$$

At last, the residual stresses in the nth layer can be expressed based on the changes of the measured strains:

$$\sigma_x^n = \frac{E'\left(\Delta\varepsilon_{mx}^n + \mu \cdot \Delta\varepsilon_{my}^n\right) \cdot (H + h_n)^2}{h_n \cdot (2 \cdot H - h_n)} \quad , \tag{26}$$

$$\sigma_y^n = \frac{E'\left(\Delta\varepsilon_{my}^n + \mu \cdot \Delta\varepsilon_{mx}^n\right) \cdot (H + h_n)^2}{h_n \cdot (2 \cdot H - h_n)} \quad . \tag{27}$$

So far, only the residual stresses in the pre-equilibrium state in the nth layer have been derived.

Using the obtained stress values in the nth layer and the thickness of the nth layer, the residual stresses in the $(n-1)$th layer can now be obtained. A schematic of the workpiece before the removal of the $(n-1)$th layer is shown in Fig. 7.

In the equilibrium state, the stresses in the neutral layer can be formulated as:

$$\sigma_{xx0}^{n-1} = -\frac{\sigma_x^n \cdot h_n + \sigma_x^{n-1} \cdot h_{n-1}}{H + h_n + h_{n-1}} \quad , \tag{28}$$

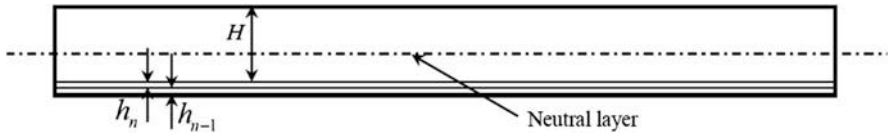

FIG. 7. Schematic of the workpiece with the last unremoved two layers.

$$\sigma_{yy0}^{n-1} = -\frac{\sigma_y^n \cdot h_n + \sigma_y^{n-1} \cdot h_{n-1}}{H + h_n + h_{n-1}} \quad . \tag{29}$$

Here σ_x^{n-1}, σ_y^{n-1} are the residual stresses in the $(n-1)$th layer in the pre-equilibrium state, and the corresponding strains in the neutral layer can be written as:

$$\varepsilon_{xx0}^{n-1} = \frac{1}{E}\left(\sigma_{xx0}^{n-1} - \mu \cdot \sigma_{yy0}^{n-1}\right) \quad , \tag{30}$$

$$\varepsilon_{yy0}^{n-1} = \frac{1}{E}\left(\sigma_{yy0}^{n-1} - \mu \cdot \sigma_{xx0}^{n-1}\right) \quad . \tag{31}$$

Using the same method, finally, the residual stress values in pre-equilibrium state in the $(n-1)$th layer can be formulated:

$$\sigma_x^{n-1} = \frac{-E' \cdot \left[\left(\Delta\varepsilon_{mx}^n + \Delta\varepsilon_{mx}^{n-1}\right) + \mu \cdot \left(\Delta\varepsilon_{my}^n + \Delta\varepsilon_{my}^{n-1}\right)\right] \cdot \left(H + h_n + h_{n-1}\right)^2 - \sigma_x^n \cdot h_n \cdot (4H + h_n + 4h_{n-1})}{h_{n-1} \cdot (4 \cdot H - 2 \cdot h_n + h_{n-1})} \quad , \tag{32}$$

$$\sigma_y^{n-1} = \frac{-E' \cdot \left[\left(\Delta\varepsilon_{my}^n + \Delta\varepsilon_{my}^{n-1}\right) + \mu \cdot \left(\Delta\varepsilon_{mx}^n + \Delta\varepsilon_{mx}^{n-1}\right)\right] \cdot \left(H + h_n + h_{n-1}\right)^2 - \sigma_y^n \cdot h_n \cdot (4H + h_n + 4h_{n-1})}{h_{n-1} \cdot (4 \cdot H - 2 \cdot h_n + h_{n-1})} \quad . \tag{33}$$

Here $\Delta\varepsilon_{mx}^{n-1}$ and $\Delta\varepsilon_{my}^{n-1}$ are the changes of the measured strains after the removal of the $(n-1)$th layer and h_{n-1} is the thickness of the $(n-1)$th layer.

As presented above, the measurement of the residual stresses in each layer is based on the changes of the measured strains and the stress values in the layers removed after it. A schematic of the workpiece before the removal of the Nth layer is shown in Fig. 8.

Before removing the Nth layer, the stresses and strains in different directions in the neutral layer can be formulated as:

$$\sigma_{xx0}^N = -\frac{\sigma_x^n \cdot h_n + \sigma_x^{n-1} \cdot h_{n-1} + \cdots + \sigma_x^N \cdot h_N}{H + h_n + h_{n-1} + \cdots + h_N} \quad , \tag{34}$$

$$\sigma_{yy0}^N = -\frac{\sigma_y^n \cdot h_n + \sigma_y^{n-1} \cdot h_{n-1} + \cdots + \sigma_y^N \cdot h_N}{H + h_n + h_{n-1} + \cdots + h_N} \quad , \tag{35}$$

$$\varepsilon_{xx0}^N = \frac{1}{E}\left(\sigma_{xx0}^N - \mu \cdot \sigma_{yy0}^N\right) \quad , \tag{36}$$

$$\varepsilon_{yy0}^N = \frac{1}{E}\left(\sigma_{yy0}^N - \mu \cdot \sigma_{xx0}^N\right) \quad . \tag{37}$$

Here σ_x^p and σ_y^p are the residual stresses in x and y directions in the Pth layer in the pre-equilibrium state, and h_P is the thickness of the Pth layer. The curvatures of the workpiece in x, y directions are defined as ρ_x^N, ρ_y^N, respectively. Now the strains through the thickness of the workpiece can be formulated:

$$\varepsilon_x^N(z) = \rho_x^N \cdot z + \varepsilon_{xx0}^N \quad , \tag{38}$$

$$\varepsilon_y^N(z) = \rho_y^N \cdot z + \varepsilon_{yy0}^N \quad . \tag{39}$$

In the equilibrium state, the stress values in the nth layer are:

$$\sigma_x^N(z)' = \sigma_x^n + E'\left[\varepsilon_x^N(z) + \mu \cdot \varepsilon_y^N(z)\right] \quad , \tag{40}$$

$$\sigma_y^N(z)' = \sigma_y^n + E'\left[\varepsilon_y^N(z) + \mu \cdot \varepsilon_x^N(z)\right] \quad . \tag{41}$$

The stress values in the $(n-1)$th layer are:

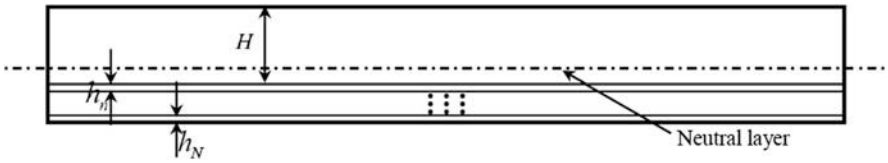

FIG. 8. Schematic of the workpiece with the last N unremoved layers.

$$\sigma_x^N(z)' = \sigma_x^{n-1} + E'\left[\varepsilon_x^N(z) + \mu \cdot \varepsilon_y^N(z)\right] \quad , \tag{42}$$

$$\sigma_y^N(z)' = \sigma_y^{n-1} + E'\left[\varepsilon_y^N(z) + \mu \cdot \varepsilon_x^N(z)\right] \quad . \tag{43}$$

The stress values in the Nth layer are:

$$\sigma_x^N(z)' = \sigma_x^N + E'\left[\varepsilon_x^N(z) + \mu \cdot \varepsilon_y^N(z)\right] \quad , \tag{44}$$

$$\sigma_y^N(z)' = \sigma_y^N + E'\left[\varepsilon_y^N(z) + \mu \cdot \varepsilon_x^N(z)\right] \quad . \tag{45}$$

The stress values through the thickness of the remaining part of the workpiece are:

$$\sigma_x^N(z)' = E'\left[\varepsilon_x^N(z) + \mu \cdot \varepsilon_y^N(z)\right] \quad , \tag{46}$$

$$\sigma_y^N(z)' = E'\left[\varepsilon_y^N(z) + \mu \cdot \varepsilon_x^N(z)\right] \quad . \tag{47}$$

Here, the value of z is $-\frac{H-h_n-h_{n-1}-\cdots-h_N}{2} \le z \le \frac{H+h_n+h_{n-1}+\cdots+h_N}{2}$.

In the equilibrium state, the total bending moments in the workpiece caused by the residual stresses are 0 in different directions, which can be expressed as:

$$M_x^N = \int_{-\frac{H+h_n+h_{n-1}+\cdots+h_N}{2}}^{\frac{H+h_n+h_{n-1}+\cdots+h_N}{2}} \sigma_x^N(z)' \cdot z \cdot \mathrm{d}z = 0 \quad , \tag{48}$$

$$M_y^N = \int_{-\frac{H+h_n+h_{n-1}+\cdots+h_N}{2}}^{\frac{H+h_n+h_{n-1}+\cdots+h_N}{2}} \sigma_y^N(z)' \cdot z \cdot \mathrm{d}z = 0 \quad . \tag{49}$$

According to the Eqs. (40)–(47), the bending moments can also be expressed as:

$$\begin{aligned} M_x^N = & \int_{-\frac{H+h_n+h_{n-1}+\cdots+h_N}{2}}^{-\frac{H-h_n+h_{n-1}+\cdots+h_N}{2}} \sigma_x^n \cdot z \cdot \mathrm{d}z + \int_{-\frac{H-h_n+h_{n-1}+\cdots+h_N}{2}}^{-\frac{H-h_n-h_{n-1}+\cdots+h_N}{2}} \sigma_x^{n-1} \cdot z \cdot \mathrm{d}z \\ & + \cdots + \int_{-\frac{H-h_n-h_{n-1}-\cdots+h_N}{2}}^{-\frac{H-h_n-h_{n-1}-\cdots-h_N}{2}} \sigma_x^N \cdot z \cdot \mathrm{d}z + \int_{-\frac{H+h_n+h_{n-1}+\cdots+h_N}{2}}^{\frac{H+h_n+h_{n-1}+\cdots+h_N}{2}} E'\left[\varepsilon_x^N(z) + \mu \cdot \varepsilon_y^N(z)\right] \cdot z \cdot \mathrm{d}z = 0 \quad , \end{aligned} \tag{50}$$

$$\begin{aligned} M_y^N = & \int_{-\frac{H+h_n+h_{n-1}+\cdots+h_N}{2}}^{-\frac{H-h_n+h_{n-1}+\cdots+h_N}{2}} \sigma_y^n \cdot z \cdot \mathrm{d}z + \int_{-\frac{H-h_n+h_{n-1}+\cdots+h_N}{2}}^{-\frac{H-h_n-h_{n-1}+\cdots+h_N}{2}} \sigma_y^{n-1} \cdot z \cdot \mathrm{d}z \\ & + \cdots + \int_{-\frac{H-h_n-h_{n-1}-\cdots+h_N}{2}}^{-\frac{H-h_n-h_{n-1}-\cdots-h_N}{2}} \sigma_y^N \cdot z \cdot \mathrm{d}z + \int_{-\frac{H+h_n+h_{n-1}+\cdots+h_N}{2}}^{\frac{H+h_n+h_{n-1}+\cdots+h_N}{2}} E'\left[\varepsilon_y^N(z) + \mu \cdot \varepsilon_x^N(z)\right] \cdot z \cdot \mathrm{d}z = 0 \quad . \end{aligned} \tag{51}$$

Based on the above, the relationship between the curvatures of the workpiece before the removal of the Nth layer and the stresses in x and y directions in different layers in the pre-equilibrium state are:

$$\begin{aligned} & E' \cdot \left(\rho_x^N + \mu \cdot \rho_y^N\right) \cdot (H + h_n + h_{n-1} + \cdots + h_N)^3 \\ & = 6 \cdot \sigma_x^n \cdot h_n \cdot (H + h_{n-1} + h_{n-2} + \cdots + h_N) \\ & + 6 \cdot \sigma_x^{n-1} \cdot h_{n-1} \cdot (H - h_n + h_{n-2} + \cdots + h_N) \\ & + \cdots + 6 \cdot \sigma_x^N \cdot h_N \cdot (H - h_n - h_{n-1} - \cdots - h_{N+1}) \quad , \end{aligned} \tag{52}$$

$$\begin{aligned} & E' \cdot \left(\rho_y^N + \mu \cdot \rho_x^N\right) \cdot (H + h_n + h_{n-1} + \cdots + h_N)^3 \\ & = 6 \cdot \sigma_y^n \cdot h_n \cdot (H + h_{n-1} + h_{n-2} + \cdots + h_N) \\ & + 6 \cdot \sigma_y^{n-1} \cdot h_{n-1} \cdot (H - h_n + h_{n-2} + \cdots h_N) \\ & + \cdots + 6 \cdot \sigma_y^N \cdot h_N \cdot (H - h_n - h_{n-1} - \cdots - h_{N+1}) \quad . \end{aligned} \tag{53}$$

The changes of the measured strains after the removal of the Nth layer can be formulated as:

$$\begin{aligned} \Delta\varepsilon_{mx}^N = & -\frac{\rho_x^N \cdot (H + h_n + h_{n-1} + \cdots + h_N)}{2} \\ & - \varepsilon_{xx0}^N - \Delta\varepsilon_{mx}^n - \Delta\varepsilon_{mx}^{n-1} - \cdots - \Delta\varepsilon_{mx}^{N+1} \quad , \end{aligned} \tag{54}$$

$$\begin{aligned} \Delta\varepsilon_{my}^N = & -\frac{\rho_y^N \cdot (H + h_n + h_{n-1} + \cdots + h_N)}{2} \\ & - \varepsilon_{yy0}^N - \Delta\varepsilon_{my}^n - \Delta\varepsilon_{my}^{n-1} - \cdots - \Delta\varepsilon_{my}^{N+1} \quad . \end{aligned} \tag{55}$$

The curvatures of the workpiece after the removal of the Nth layer can be derived based on the changes of the measured strains:

$$\rho_x^N = \frac{-2\left(\varepsilon_{xx0}^N + \Delta\varepsilon_{mx}^n + \Delta\varepsilon_{mx}^{n-1} + \cdots + \Delta\varepsilon_{mx}^N\right)}{H + h_n + h_{n-1} + \cdots + h_N} \quad , \quad (56)$$

$$\rho_y^N = \frac{-2\left(\varepsilon_{yy0}^N + \Delta\varepsilon_{my}^n + \Delta\varepsilon_{my}^{n-1} + \ldots + \Delta\varepsilon_{my}^N\right)}{H + h_n + h_{n-1} + \ldots + h_N} \quad . \quad (57)$$

Using Eqs. (52) and (53), the stress values in the Nth layer can be obtained as:

$$\sigma_x^N = \frac{M_x^N + J_x^n(N) + J_x^{n-1}(N) + \cdots + J_x^{n-m}(N) + \cdots + J_x^{N+1}(N)}{P^N} \quad (58)$$

$$\sigma_y^N = \frac{M_y^N + J_y^n(N) + J_y^{n-1}(N) + \cdots + J_y^{n-m}(N) + \cdots + J_y^{N+1}(N)}{P^N} \quad , \quad (59)$$

where

$$M_x^N = -E' \cdot \left[\left(\Delta\varepsilon_{mx}^n + \Delta\varepsilon_{mx}^{n-1} + \cdots + \Delta\varepsilon_{mx}^N\right) + \mu \cdot \left(\Delta\varepsilon_{my}^n + \Delta\varepsilon_{my}^{n-1} + \cdots + \Delta\varepsilon_{my}^N\right)\right] \cdot (H + h_n + h_{n-1} + \cdots + h_N)^2$$

$$P^N = h_N \cdot (4 \cdot H - 2 \cdot h_n - 2 \cdot h_{n-1} - \cdots - 2 \cdot h_{N+1} + h_N)$$

$$J_x^n(N) = -\sigma_x^n \cdot h_n \cdot (4 \cdot H + h_n + 4 \cdot h_{n-1} + \cdots + 4 \cdot h_N)$$

$$J_x^{n-1}(N) = -\sigma_x^{n-1} \cdot h_{n-1} \cdot (4 \cdot H - 2 \cdot h_n + h_{n-1} + 4 \cdot h_{n-2} + \cdots + 4 \cdot h_N)$$

$$\cdots$$

$$J_x^{n-m}(N) = -\sigma_x^{n-m} \cdot h_{n-m} \cdot (4 \cdot H - 2 \cdot h_n - \cdots - 2 \cdot h_{n-m+1} + h_{n-m} + 4 \cdot h_{n-m-1} + \cdots + 4 \cdot h_N)$$

$$\cdots$$

$$J_x^{N+1}(N) = -\sigma_x^{N+1} \cdot h_{N+1} \cdot (4 \cdot H - 2 \cdot h_n - \cdots - 2 \cdot h_{N+2} + h_{N+1} + 4 \cdot h_N) M_y^N = -E' \cdot \left[\left(\Delta\varepsilon_{my}^n + \Delta\varepsilon_{my}^{n-1} + \cdots + \Delta\varepsilon_{my}^N\right) + \mu \cdot \left(\Delta\varepsilon_{mx}^n + \Delta\varepsilon_{mx}^{n-1} + \cdots + \Delta\varepsilon_{mx}^N\right)\right] \cdot (H + h_n + h_{n-1} + \cdots + h_N)^2$$

$$J_y^n(N) = -\sigma_y^n \cdot h_n \cdot (4 \cdot H + h_n + 4 \cdot h_{n-1} + 4 \cdot h_{n-2} + \cdots + 4 \cdot h_N)$$

$$J_y^{n-1}(N) = -\sigma_y^{n-1} \cdot h_{n-1} \cdot (4 \cdot H - 2 \cdot h_n + h_{n-1} + 4 \cdot h_{n-2} + \cdots + 4 \cdot h_N)$$

$$\cdots$$

$$J_y^{n-m}(N) = -\sigma_y^{n-m} \cdot h_{n-m} \cdot (4 \cdot H - 2 \cdot h_n - \cdots - 2 \cdot h_{n-m+1} + h_{n-m} + 4 \cdot h_{n-m-1} + \cdots + 4 \cdot h_N)$$

$$\cdots$$

$$J_y^{N+1}(N) = -\sigma_y^{N+1} \cdot h_{N+1} \cdot (4 \cdot H - 2 \cdot h_n - \cdots - 2 \cdot h_{N+2} + h_{N+1} + 4 \cdot h_N) \quad .$$

Now, the residual stresses in all layers can be calculated. The obtained stress values using the method above are in the pre-equilibrium state. Therefore, the effects of the workpiece's rigidity were neglected.

III. EXPERIMENTAL PROCESS

A. Machining process

The unmachined workpiece is shown in Fig. 9(a). The material is Ti6Al4V. The length, width, and the depth of the workpiece are 170, 20, and 6 mm, respectively. To rule out the effects of internal residual stresses on the measured results, the workpiece was

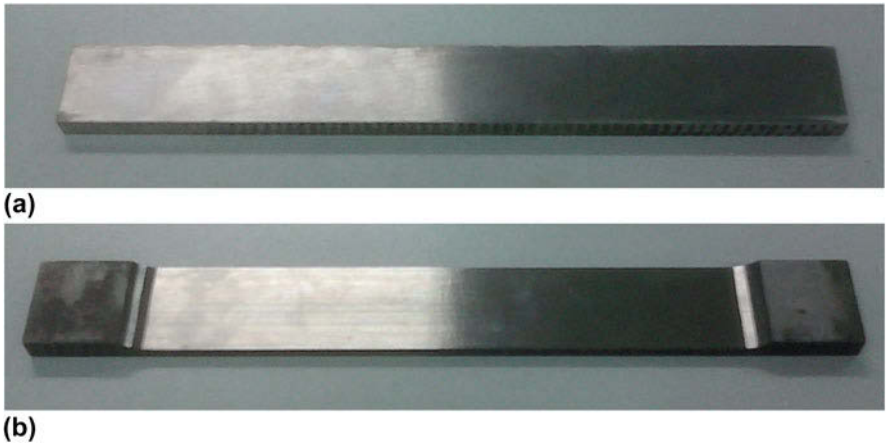

FIG. 9. (a) The workpiece before machining. (b) The workpiece after machining.

annealed to remove most of the internal residual stresses before machining.

The schematic of clamping the workpiece during the machining process is as shown in Fig. 10. The workpiece was milled using a cylinder-milling tool with four blades. The diameter of the milling tool was 11 mm. The parameters used for the last cut are: cutting speed v_c = 35 m/min, feed rate per tooth f_z = 0.04 mm/z, radial cutting depth a_e = 1 mm, axial cutting depth a_p = 20 mm, the milled workpiece is as shown in Fig. 9(b). The thickness of the milled part is 1.2 mm.

B. Layer removal via chemical corrosion

To measure the residual stresses throughout the thickness of the stress layer, we used chemical polishing to remove material layer by layer. Hydrofluoric acid (HF) was chosen as corrosive, the nitric acid (HNO_3) was chosen as oxidizing agent to prevent the generation of hydrogen to improve the surface property.[17,18]

During the chemical polishing, the opposite side of the milled surface was protected with 704 silicone. The thickness of each removed layer was controlled via the polishing time. The accurate value of each removed layer thickness was determined using a thickness gauge with an accuracy of 1 μm.

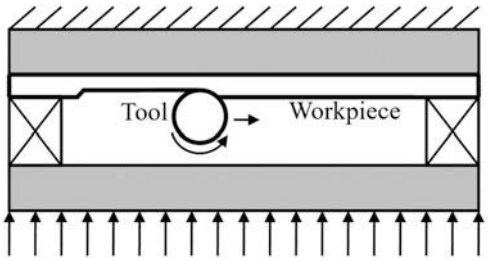

FIG. 10. Schematic, illustrating the clamping of the workpiece during the machining process.

C. Measurement of the strain changes

To measure the strain changes after each layer removal, the strain gauges were attached to the surface opposite the milled surface—see Fig. 11. The strain gauges were half-bridge connected to compensate the temperature effects during the experiment.

D. Measured results

Based on the measured strain changes, the surface residual stresses generated by milling were calculated using Eqs. (26), (27), (58), and (59). The residual stresses as a function of depth into the workpiece are shown in Fig. 12. It can be seen that both the residual stresses in the cutting and transverse directions are compressive in the outmost layer. The highest stress in the cutting direction is about −175 MPa, and the highest stress in the transverse direction is about −150 MPa. At the depth around 60 μm, however, the stresses in both directions are very small and can be neglected. The stresses in cutting direction are slightly higher than that in the transverse direction.

IV. THE FINITE ELEMENT MODEL

To validate the measured stress values, we created a finite element model in the software of Abaqus that represents the real workpiece. At last, 108,800 elements were generated in the model, and the type of the element used is C3D8R. The measured stress values were loaded into the model. The model in pre-equilibrium state is as shown in Figs. 13(a) and (b). So far, the residual stresses have not caused any deformations of the workpiece. Therefore, the residual stresses have not been redistributed

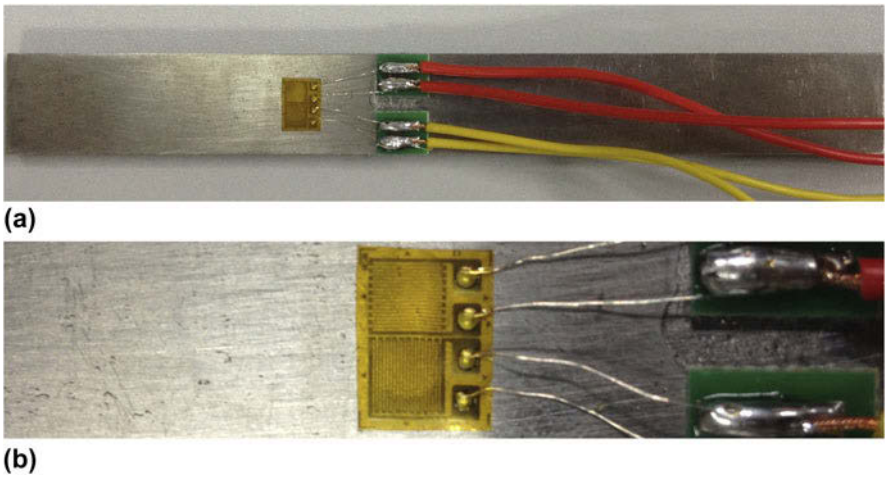

FIG. 11. (a) The workpiece with the strain gauges attached. (b) The strain gauges attached to the workpiece.

yet. Only the movement along the z direction of both ends of the model was restricted. Therefore, the model can bend freely and the strains in x and y directions can be read easily in the model. Because the residual stress values are far below the elastic limit of the material, only the elastic modulus and Poisson's ratio of the material were defined: E = 108,000 MPa, μ = 0.34. After the equilibrium state had been obtained, the workpiece was deformed—see Fig. 13(c). The residual stresses input into the model were redistributed as shown in Fig. 13(d). The highest Von Mises stress in the equilibrium state is about 54% of the pre-equilibrium state.

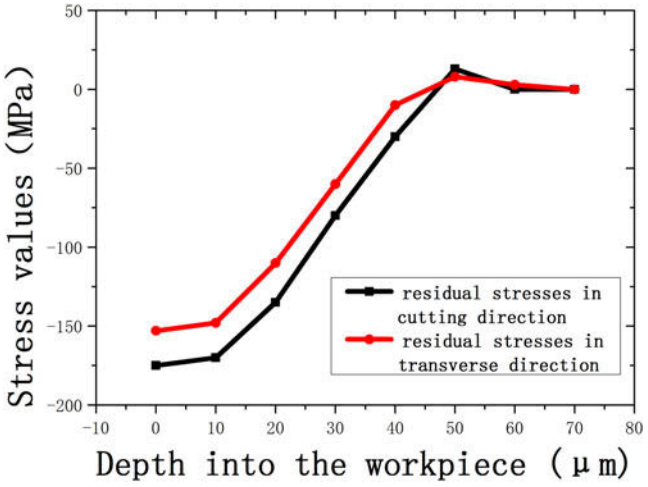

FIG. 12. The measured surface residual stresses induced by milling.

Comparisons of the residual stresses in different states are shown in Fig. 14. The highest stress in the equilibrium state in the cutting direction is about 51% of that in the pre-equilibrium state. On the other hand, the highest value of the stress in equilibrium state in the transverse direction is about 54% of that in the pre-equilibrium state.

Overall, the distribution of the residual values had changed a lot after the equilibrium state was reached. The distributions of the surface residual stresses in the equilibrium state are very different from that in the pre-equilibrium state, which is always significantly affected by the rigidity of the workpiece. Because the stress values obtained via XRD are always the values in the equilibrium state, the measured stress values in the workpieces with different rigidities are expected to be different.

The elements in each layer were eliminated ("killed") layer by layer with the technology of element birth and death to simulate the process of layer removal in the experiments. After each layer removal, the equilibrium state of the residual stresses is perturbed and a new equilibrium state is reached. There are some strain

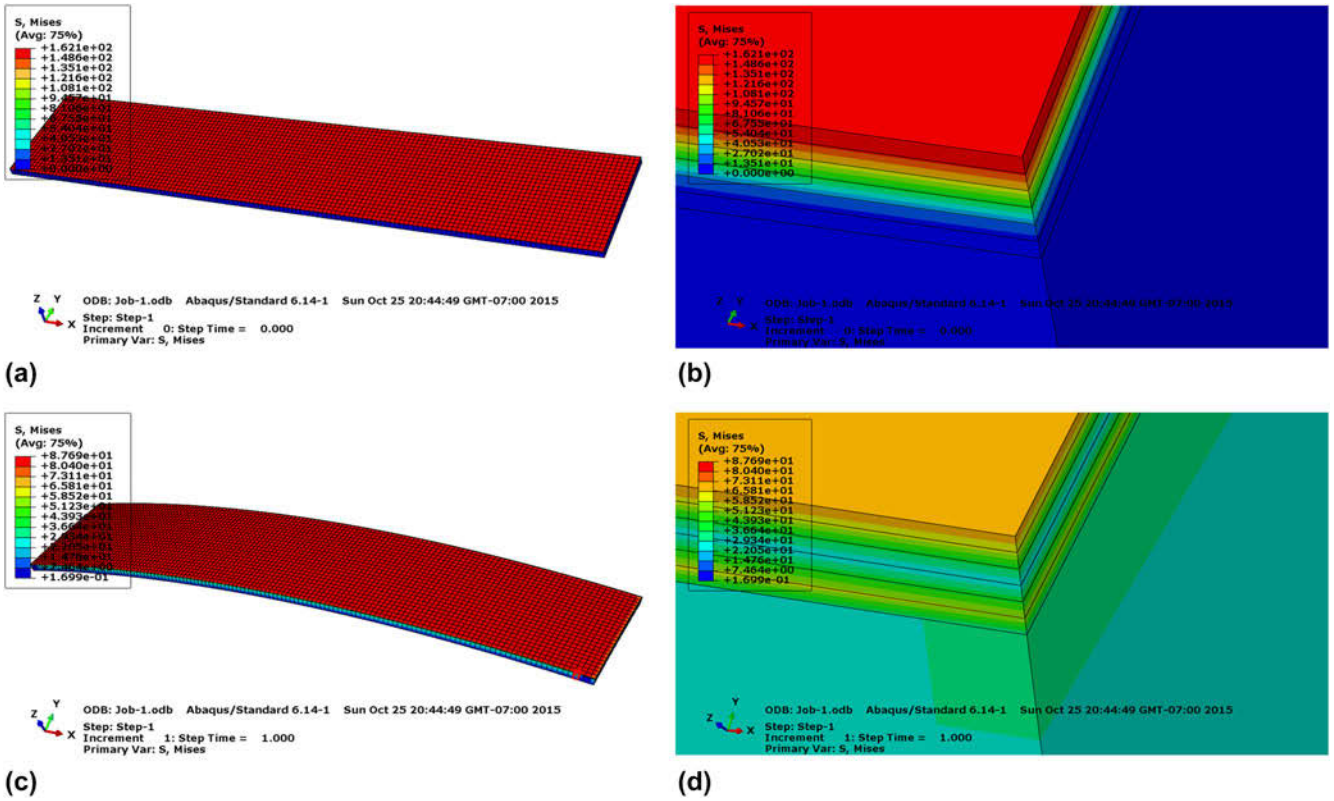

FIG. 13. (a) The whole model in the pre-equilibrium state. (b) Part of the model in the pre-equilibrium state. (c) The whole model in the equilibrium state. (d) Part of the model in the equilibrium state.

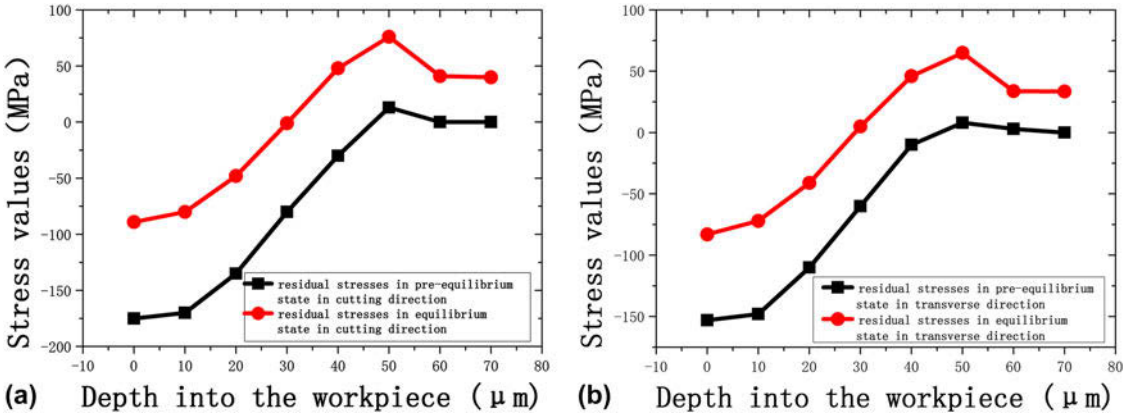

FIG. 14. (a) The surface residual stresses in cutting direction. (b) The surface residual stresses in transverse direction.

changes on the surface opposite the milled surface. The strain changes derived from the finite element model after removal of each layer were compared to the measured experimental values. The maximum error was about 0.8%, which indicated that the strains obtained from the two different methods are in good agreement. The remaining small deviation may be attributed to the meshes in the finite element model not being fine enough. Overall, the finite element analysis successfully validates the stress values from the experimental results.

V. CONCLUSIONS

We described and investigated a method for measuring the surface residual stresses caused by milling. It is based on the strain changes on the surface opposite the milled surface in combination with the inverse calculation. A finite element model was used to validate the measured values. Our conclusions can be summarized as follows:

(1) The residual stress values were calculated from the last removed layer to the first removed layer. It is necessary to consider the changed position of the neutral layer as well as the changed deformation of the workpiece caused by the changed neutral layer and the residual stresses in the remaining layers.

(2) The distribution of the residual stresses in the pre-equilibrium state is very different from that in the equilibrium state. To predict the deformations of different workpieces, especially for workpieces with poor rigidity, it is necessary to measure the residual stresses in the pre-equilibrium state.

(3) According to our measured results, the residual stresses induced by milling in the Ti6Al4V workpiece are compressive in both the cutting direction and transverse direction. The stress values in the cutting direction are slightly higher than those in the transverse direction are. At a depth of about 60 μm, the stress values in both directions are close to zero.

(4) As validated by the finite element analysis, the strain changes obtained from the two different methods are in good agreement. This indicates that the results obtained from the measuring technique described in this paper are correct. We can conclude that the measuring method accurately determines the surface residual stresses caused by milling. It can be a very useful tool to provide one reliable indicator for evaluating the machined surface properties.

ACKNOWLEDGMENTS

Part of this work was supported by the National Natural Science Foundation of China (No. 51405226) and Natural Science Foundation of Jiangsu Province (No. SBK2014043631).

REFERENCES

1. J.J. Wang, S.Z. Shang, G.M. Lu, and J.G. Yu: Viscosity estimation of semi-solid alloys based on thermal simulation compression tests. *Int. J. Mater. Res.* **104**, 255 (2013).
2. J.J. Wang, D. Brabazon, A.B. Phillion, and G.M. Lu: An innovative two-stage reheating process for wrought aluminum alloy during thixoforming. *Metall. Mater. Trans. A* **46**, 4191 (2015).
3. V.G. Navas, O. Gonzalo, and I. Bengoetxea: Effect of cutting parameters in the surface residual stresses generated by turning in AISI 4340 steel. *Int. J. Mach. Tools Manuf.* **61**, 48 (2012).
4. M. Sebastiani, C. Eberl, E. Bemporad, and G.M. Pharr: Depth-resolved residual stress analysis of thin coatings by a new FIB–DIC method. *Mater. Sci. Eng., A* **528**, 7901 (2011).
5. A.K. Mainjot, G.S. Schajer, A.J. Vanheusden, and M.J. Sadoun: Residual stress measurement in veneering ceramic by hole-drilling. *Dent. Mater.* **27**, 439 (2011).
6. E. Carrera, A. Rodríguez, J. Talamantes-Silva, D. Gloria, S. Valtierra, and R. Colás: Study of residual stresses in complex aluminium castings. *Int. J. Cast Met. Res.* **25**, 264 (2012).
7. N.S. Rossini, M. Dassisti, K.Y. Benyounis, and A.G. Olabi: Methods of measuring residual stresses in components. *Mater. Des.* **35**, 572 (2012).
8. P.J. Arrazola, A. Kortabarria, A. Madariaga, J.A. Esnaola, E. Fernandez, C. Cappellini, D. Ulutan, and T. Özel: On the machining induced residual stresses in IN718 nickel-based alloy: Experiments and predictions with finite element simulation. *Simulat. Model. Pract. Theor.* **41**, 87 (2014).

9. A. Singh and A. Agrawal: Investigation of surface residual stress distribution in deformation machining process for aluminum alloy. *J. Mater. Process. Technol.* **225**, 195 (2015).
10. P. Mann, H.Y. Miao, A. Gariépy, M. Lévesque, and R.R. Chromik: Residual stress near single shot peening impingements determined by nanoindentation and numerical simulations. *J. Mater. Sci.* **50**, 2284 (2015).
11. E. Brinksmeier and J. Sölter: Prediction of shape deviations in machining. *CIRP Ann.—Manuf. Technol.* **58**, 507 (2009).
12. L. Meng, N. He, L. Li, Y. Yang, and W. Zhao: Measurement of the residual stress induced by milling in TC4 workpiece before self-balancing and its FEA. *Rare Metal Mater. Eng.* **43**, 1991 (2014).
13. L. Meng, N. He, Y. Yang, and W. Zhao: Measurement of surface residual stresses generated by turning thin-wall Ti6Al4V tubes using different cutting parameters. *Rare Metal Mater. Eng.* **44**, 2381 (2015).
14. L. Meng, N. He, and L. Li: Calculation of residual stress induced by machining in internal surface of TC4 tubular parts and its FEA. *China Mech. Eng.* **25**, 2583 (2014).
15. L. Meng, N. He, Y. Yang, W. Zhao, and B. Rong: Method for measuring residual stresses induced by boring in internal surface of tube and its validation with XRD method. *Trans. Nanjing Univ. Aeronaut. Astronaut.* **31**, 508 (2014).
16. L. Meng, N. He, Y. Yang, and W. Zhao: Application of FEM correction to measuring the surface residual stresses generated by turning Ti6Al4V tube parts. *J. Harbin Inst. Technol.* **47**, 71 (2015).
17. M. Yin, G. Liao, Q. Wen, and H. Cheng: Chemical milling process for 2219 aluminum alloy tube. *Mater. Prot.* **38**, 24 (2006).
18. X. Zhu, L. Wu, and H. Zheng: The analytic method of Nat S in chemical milling solution. *Mater. Coat. Electroplating* **4**, 40 (2006).